JOURNAL OF THEORETICAL AND APPLIED MECHANICS
56, 3, pp. 601-614, Warsaw 2018
DOI: 10.15632/jtam-pl.56.3.601

COARSE-GRAINING MODELS FOR MOLECULAR DYNAMICS SIMULATIONS OF FCC METALS

Pourya Delafrouz, Hossein Nejat Pishkenari
Department of Mechanical Engineering, Sharif University of Technology, Tehran, Islamic Republic of Iran
e-mail: nejat@sharif.edu

In this paper, four coarse-graining (CG) models are proposed to accelerate molecular dynamics simulations of FCC metals. To this aim, at first, a proper map between beads of the CG models and atoms of the all-atom (AA) system is assigned, afterwards mass of the beads and the parameters of the CG models are determined in a manner that the CG models and the original all-atom model have the same physical properties. To evaluate and compare precision of these four CG models, different static and dynamic simulations are conducted. The results show that these CG models are at least 4 times faster than the AA model, while their errors are less than 1 percent.

Keywords: accelerated molecular dynamics, coarse-grain models, FCC metals, EAM potential

1. Introduction

One of the important challenges of working at the nanoscale is to analyze materials properties. Because experimental researches in characterization and analysis of materials characteristics at nano-scale are significantly expensive, improvement of theoretical modeling methods is an in-progress research field. Also, there are some important subjects which experimental setups and techniques cannot capture. On the other hand, it seems necessary to assess the system behavior and amend the experimental setup based on the results of modeling and simulation techniques before any practical attempt. Consequently, computational modelling techniques, with their great potential to model and predict atomic features of nano-structures, entice the interest of many researchers in nanotechnology. The necessity for this predictive capability has empowered computational modeling and simulation methods to become an important component for inspecting phenomena in different nano-scale engineering applications. The most popular computational methods used in simulations at micro and nano scales are classic and non-classic continuum theories (Chandramouli, 2014), molecular dynamics (MD) (Leach, 2001; Muc, 2011) and Monte-Carlo (Berg, 2005; Samani and Pourtakdoust, 2014). Molecular dynamics (MD) is a powerful technique in the computational study of nano-scale structures and processes, which can provide data on the time dependent performance of a molecular system.

Augmented by quantum mechanical computations of interatomic potentials that explain the interaction of atoms, molecular dynamics can model behavior of a variety of materials with all-atom detail. However, the all-atom (AA) molecular dynamics method is not able to model many phenomena because it is practically limited to system sizes less than a few tens of nanometers and simulation times less than a few hundreds of nanoseconds (Chen *et al.*, 2011). These restrictions have attracted a lot of attention in the development of techniques to accelerate molecular dynamics simulations. To accelerate long-time molecular simulations, different methods including increasing the integration time step, reducing the computational cost per step, or combinations of these methodologies have been developed (Poursina and Anderson, 2014). These improvements may be achieved through clustering atoms to make a larger rigid

bead or by employing continuum theories in combination with atomistic modeling. Totally, there are two main schemes for accelerating molecular dynamics simulations: multi-scale modeling (Cranford and Buchler, 2010; Park and Klein, 2007; Jovanovic and Filipovic, 2006) and coarse--graining (CG) methods (Ouldridge, 2012; Yang and Ou, 2014; Hedrich and Hedrich, 2010).

As noted by Yang and To (2015), numerous multiscale techniques have been proposed to achieve the accuracy of full atomistic simulations with a reduced computational cost (Tadmor *et al.*, 2013; Burbery *et al.*, 2017). These methods couple atomistic and continuum models to link different spatial and time scales from nanometer and femtosecond to meter and second (Paćko and Uhl, 2011; Karma and Tourret, 2016).

FCC metals are commonly used in MEMs/NEMs systems as a main material. Although there exists a lot of researches employing the molecular dynamics technique for the modeling of FCC metals (Pishkenari and Meghdari, 2010; Lao *et al.*, 2013; Pishkenari, 2015), faster techniques with enough accuracy are highly demanded for modeling these metals (Park and Klein, 2007; Oren *et al.*, 2016).

In this paper, we have proposed four effective CG models based on the first technique introduced in the previous paragraph, for simulation of FCC metals. To this aim, at first, the proper atomic structure is defined and based on this new atomic structure, mass of the beads is determined. Then, the potential parameters are determined in a manner that the original model and the coarse-grained models have the same physical properties like cohesive energy, bulk modulus and elastic constants. After developing CG models, the bulk properties of an FCC metal such as elastic constants, bulk modulus and potential energy are determined and compared with the results of the AA model. As a case-study, to show the speed and accuracy of the developed coarse-graining models in prediction of mechanical properties of nano-scale systems, we have studied longitudinal and transversal vibrations of nanowires. The results demonstrate that the error of the CG models is reduced when the surface effects decrease.

The main goal of this paper is introduction of a novel coarse-grain model in order to accelerate the molecular dynamics simulations. The way of implementing these methods for modeling of nanowires are as same as using the molecular dynamics method with few changes. Owing to decreasing the number of beads in these methods, nanowires of larger size can be modeled with better accuracy compared to the Finite Element model. As an example, the error of calculating the natural transversal frequency among the all-atom model and one of the CG model is less than 0.6 percent for a nanowire with 65.28 nm length and 13.056 nm thickness while it is 4 times faster. Hence, these CG models are faster than the Molecular Dynamics method and more accurate than the Finite Element method. The rest of the paper is organized as follows. In Section 2, four CG models for analyzing FCC metals are introduced. In that Section, proper mapping, mass of beads and potential parameters are developed. In Section 3, size-dependency of the proposed models is investigated by various static and dynamic simulations. The last Section is devoted to concluding remarks.

2. Proposed CG method

The term "coarse graining" is used for methods based on replacing some atoms with one bead in order to reduce the number of degrees of freedom. Since the number of degrees of freedom in a CG model is significantly lower than in the main atomic system, simulation of the CG system needs considerably less computational resources; consequently, the simulation time and the system size can be substantially decreased (Cascella and Dal Peraro, 2009; Marrink *et al.*, 2007).

To develop a CG model for analyzing FCC metals, three steps must be done. At first, the location of the beads must be assigned. After choosing a proper atomic structure, the mass of the beads is specified and, finally, inter-atomic potential parameters are determined.

2.1. Mapping

One way to arrange the locations of beads is to choose an FCC crystalline structure as the CG model having a different lattice constant in comparison with the main atomic structure. In this way, a new FCC metal is made of the representative beads. Herein, the lattice constant of the CG model is set as twice of the lattice constant of the AA model, i.e. $a_{CG} = 2a_{AA}$, where a_{AA} and a_{CG} are respectively the lattice constants of the AA and CG models. Figure 1 shows this mapping for a cubic structure with an edge of $2a_{AA}$.

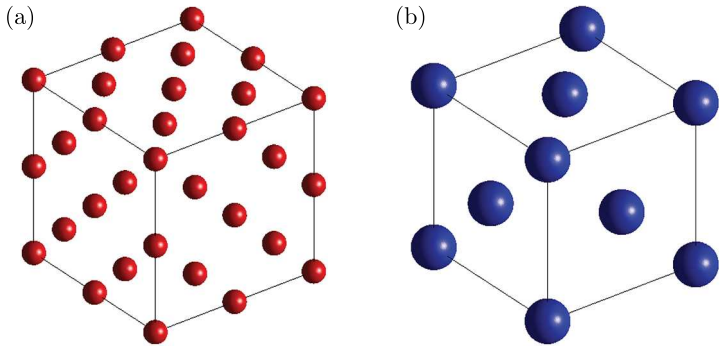

Fig. 1. 3-D display of (a) the AA model and (b) the CG model

The number of the beads in the resultant CG structure is about one-eighth of the number of atoms in the original structure. It should be mentioned that all of the four CG models have the same arrangement of the beads. After introducing the proposed mapping, the mass of the beads must be specified.

2.2. Mass of beads

By calculating contributions of each atom to the assigned beads, the mass of the beads can be determined. At first, we describe how the mass of the internal beads, named as bulk beads, can be calculated. Based on the structure of the CG and AA models, there is an atom that is in the same place where the bead is and its entire mass contributes to the corresponding bead. There are also 12 atoms surrounding the bead with a distance $(\sqrt{2}/2)a_{AA}$ from the bead and being shared with another bead equally. Also, there are 6 atoms with distance a_{AA} from the bulk bead each of which are shared among 6 beads. Consequently, the mass of the bulk bead can be calculated as below

$$M_{bulk} = \Big(1 + 12 \cdot \frac{1}{2} + 6 \cdot \frac{1}{6}\Big) m_{atom} = 8 m_{atom} \tag{2.1}$$

where m_{atom} is the atomic mass of the FCC material. In addition to bulk beads, there are other new beads including surface beads, edge beads and corner beads.

For the surface beads, there is an atom at the same place where the bead is. There are 8 atoms at the distance $(\sqrt{2}/2)a_{AA}$ from the surface bead each of which is shared between two beads. There are also 4 atoms on the surface with the distance a_{AA} from the surface bead, and they are shared among 5 beads. Also there exists one atom of the system with the distance a_{AA} from the surface bead that is shared among 6 beads. So the mass of the surface bead can be calculated as follows

$$M_{surface} = \Big(1 + 8 \cdot \frac{1}{2} + \frac{1}{6} + 4 \cdot \frac{1}{5}\Big) m_{atom} = \frac{179}{30} m_{atom} \approx 5.97 m_{atom} \tag{2.2}$$

The number of atoms with the distance $(\sqrt{2}/2)a_{AA}$ from the edge bead is 5, and each of them is shared between two beads. There are 4 atoms with the distance a_{AA} from the edge bead.

Two of them are on the surface and are shared among 4 beads while the remaining atoms are shared among 5 beads are at the edge. By noticing one atom at the same place where the edge bead is, the mass of the bead is calculated as follows

$$M_{edge} = \left(1 + 5 \cdot \frac{1}{2} + 2 \cdot \frac{1}{4} + 2 \cdot \frac{1}{5}\right) m_{atom} = 4.4 m_{atom} \tag{2.3}$$

The mass of the corner bead can be calculated as follows. There are 3 atoms that are shared between two beads with the distance $(\sqrt{2}/2)a_{AA}$ from each atom. There are also 3 atoms with the distance a_{AA} from the corner bead, and each of them are shared among 4 beads. Hence, the mass of the corner bead is obtained as follows

$$M_{corner} = \left(1 + 3 \cdot \frac{1}{2} + 3 \cdot \frac{1}{4}\right) m_{atom} = 3.25 m_{atom} \tag{2.4}$$

In addition to the four aforementioned beads, there are some new beads with different atomic neighborhood. To determine the mass of these new beads, a system is created with both AA and CG structures. Then all of atoms with the distance which is equal or less than one lattice constant from each bead are determined. Also, the number of beads, inheriting from each atom, must be calculated. With this data, mass allocation for each bead can be computed and used in MD simulations. LAMMPS software (Plimpton, 1995) is used as the main solver in our simulations.

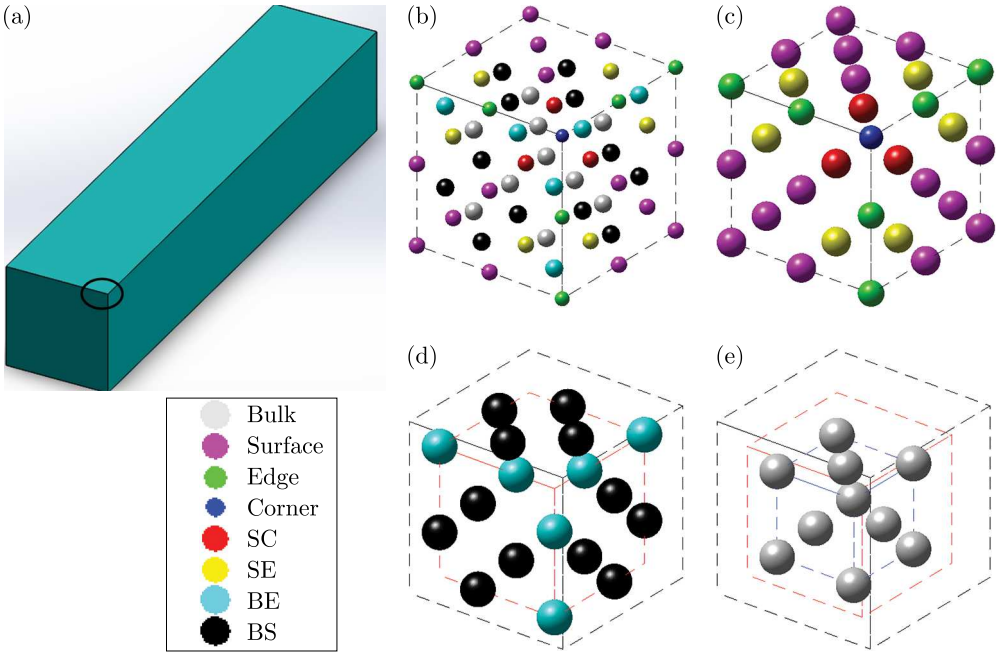

Fig. 2. Eight types of beads in the last CG model: (a) one corner of a nanowire which can be zoomed in to display different bead types, (b) a cubic box on the corner of the nanowire with the edge of $2a_{CG}$ (all types of beads are shown in this part of figure simultaneously), (c) external layer of the beads of the corner, (d) the first internal layer of the beads of the corner, (e) the second internal layer of the beads of the corner

By using the mentioned algorithm, 8 types of beads are obtained (Fig. 2). Four of them are previously mentioned as the bulk, surface, edge and corner beads. The rest of them is as follows:

- Beads shared between the surface and corner: these beads are on the surface with the distance a_{AA} from the corner and their mass is $M_{SC} = 6.0667 m_{atom}$.
- Beads shared between the surface and edge: there are beads with mass of $M_{SE} = 6.0167 m_{atom}$. These beads are on the surface with the distance a_{AA} from the edge.

- Beads shared between the bulk (internal material) and edge: these internal beads have the distance a_{AA} from the edge and their mass is $M_{BE} = 8.0667 m_{atom}$.
- Beads shared between the bulk and surface: these internal beads have the distance a_{AA} from the surface and their mass is $M_{BS} = 8.033 m_{atom}$.

Currently, we can introduce 4 CG models based on the mass assignment. Table 1 lists the specifications of these CG models. Although the second and third coarse-graining methods have the same mass assignments, their potential parameters are different (see the next Section).

Table 1. Four different CG models

CG model	Mass assignment
CG_1	One bead type: $M_{bulk} = 8m_{atom}$
CG_2	Four bead types: $M_{bulk} = 8m_{atom}$, $M_{surface} = 5.9667m_{atom}$, $M_{edge} = 4.4m_{atom}$, $M_{corner} = 3.25m_{atom}$
CG_3	Four bead types: $M_{bulk} = 8m_{atom}$, $M_{surface} = 5.9667m_{atom}$, $M_{edge} = 4.4m_{atom}$, $M_{corner} = 3.25m_{atom}$
CG_4	Eight bead types: $M_{bulk} = 8m_{atom}$, $M_{surface} = 5.9667m_{atom}$, $M_{edge} = 4.4m_{atom}$, $M_{corner} = 3.25m_{atom}$, $M_{SC} = 6.0667m_{atom}$, $M_{SE} = 6.0167m_{atom}$, $M_{BE} = 8.0667m_{atom}$, $M_{BS} = 8.033m_{atom}$

In this Section, we have introduced 8 types of beads which was developed for a cubic system. In the next Section, the potential parameters are determined for the CG models.

2.3. Potential parameters

The most widely used potential for the modeling of FCC metals is EAM (Zhou *et al.*, 2004). In this potential, the total potential energy can be expressed as

$$E = \frac{1}{2} \sum_{i,j,\, i \neq j} \varphi_{ij}(r_{ij}) + \sum_i F_i(\rho_i) \tag{2.5}$$

This potential model has two parts. The first part is φ_{ij} that is known as pair energy between atoms i and j, and the second part is embedding energy $F_i(\rho_i)$ that describes the effect of electron density ρ_i. The electron density can be obtained as below

$$\rho_i = \sum_{i,\, j \neq i} f_i(r_{ij}) \tag{2.6}$$

where $f_i(r_{ij})$ is the electron density produced by atom j at the position of atom i.

Herein, at first, the potential parameters for the first model (CG_1) is introduced. For the first model, each bead is representative of eight atoms, hence the cohesive energy per bead in the CG model should be 8 times bigger than the cohesive energy per atom in the AA model. Consequently, to have the same potential energy for both CG_1 and AA models at any arbitrary point, the potential energy obtained from Eq. (2.5) for the first CG model, must be multiplied by 8 to reproduce the correct potential energy.

On the other hand, since the lattice constant of the CG models is $a_{CG} = 2a_{AA}$, the distance between beads is also twice the distance between atoms. Thus, every part of the potential which is a function of distance, must be modified to be a function of distance divided by 2. Totally, the potential function for the first CG model, can be represented as follows

$$\varphi_{CG_1}(r_{ij}) = 8\varphi_{AA}\Big(\frac{r_{ij}}{2}\Big) \qquad \rho_{CG_1}(r_{ij}) = \rho_{AA}\Big(\frac{r_{ij}}{2}\Big) \qquad F_{CG_1}(\rho_i) = 8F_{AA}(\rho_i) \tag{2.7}$$

For the second CG model, the mass assignment for the beads is different from the first CG model; however, the potential parameters for these models are considered to be the same. For the third and fourth CG models, the potential parameters are modified based on the mass proportions. This means that each bead is not necessary representative of 8 atoms, and only bulk atoms are representative of eight atoms and other beads are representative of M_{bead}/m_{atom} atoms. Therefore, it is reasonable to replace number 8 in Eq. (2.7) with M_{bead}/m_{atom} as follows

$$\begin{aligned} &\varphi_(CG_1)(r_{ij}) = \frac{M_{bead}}{m_{atom}}\varphi_{AA}\Big(\frac{r_{ij}}{2}\Big) \qquad\qquad \rho_{CG_1}(r_{ij}) = \rho_{AA}\Big(\frac{r_{ij}}{2}\Big) \\ &F_{CG_1}(\rho_i) = \frac{M_{bead}}{m_{atom}}F_{AA}(\rho_i) \end{aligned} \tag{2.8}$$

For this model, a different pairwise potential is required for calculating the interaction between two different beads. So, the EAM potential relation for alloys can be used (Zhou *et al.*, 2004), which has the following relation

$$\varphi^{ab}(r) = \frac{1}{2}\Big[\frac{\rho^b(r)}{\rho^a(r)}\varphi^{aa}(r) + \frac{\rho^a(r)}{\rho^b(r)}\varphi^{bb}(r)\Big] \tag{2.9}$$

Equation (2.9) shows the pairwise potential function for alloys a and b. Since electron density is equal for all beads, the average of the two pairwise potential function should be considered for the interaction between two beads.

Thus, in this paper, four different CG models which have the following specifications are considered:

1. CG_1: one type of bead,
2. CG_2: four types of beads having four different mass values while using the same potential parameters,
3. CG_3: four types of beads having four different mass values and potential parameters tuned based on the mass of the beads,
4. CG_4: eight types of beads having eight different mass values and potential parameters tuned based on the mass of the beads.

After introducing the CG models, the validity of them must be checked. For this purpose, bulk simulations such as calculating elastic properties are performed firstly. In our simulations, gold is studied as one of the FCC metals. To simulate a bulk material, periodic boundary conditions are used in three dimensions to remove the effect of boundaries. A cubic central box with an edge length of $10a_{AA}$ is considered. Our goal is to compare the total potential energy, bulk modulus and elastic properties obtained from the CG models with those obtained from the AA method and experiment (Simmons and Wang, 1971). For evaluating the elastic constants, a specified strain is applied to the system and stress changes caused by the strain are measured. By dividing the stress changes by strain, different elastic constants are calculated. Generally, a material has 36 elastic constants; however, for FCC metals, due to symmetry, there are only three different elastic constants. As can be expected, our simulation results demonstrate that all CG models predict the bulk properties exactly as same as the AA model. In fact, all of the CG models behave completely similar, since for the bulk materials there exists only one bead type. Therefore, all CG models are appropriate for the modeling of the bulk FCC materials.

In the following Section, some static and dynamic simulations are performed so as to check the size-dependency of these models. To this aim, in different nanowires, the natural frequency of longitudinal and transversal vibrations by employing these models is calculated. Then the results are compared with the results of the AA model. Investigation of how accurate these CG models can predict the mechanical properties of an FCC metal having free surfaces is studied in the next Section.

3. Case study

In this Section, the accuracy of the CG models in the prediction of mechanical properties of small--size nanowires is examined. To this aim, Young's modulus in static longitudinal deformation and the natural frequency in longitudinal and transversal vibrations of nanowires are studied. Figure 3 depicts a gold nanowire with clampled-free boundary conditions.

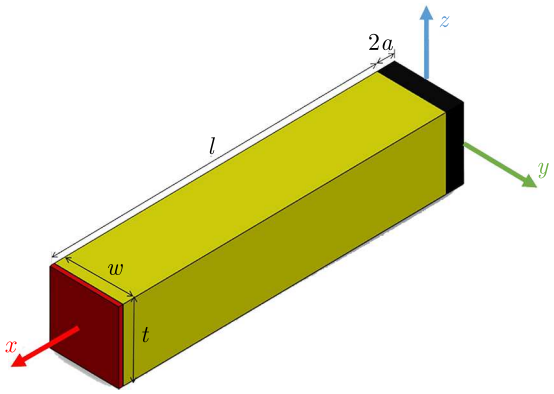

Fig. 3. A gold nanowire. Three zones are recognizable at each setup: the boundary zone having a length $2a_{AA}$ (shown by black color), moving zone having a length a_{AA} (shown by yellow color), and the excitation zone displayed in red color

3.1. Longitudinal deformation

Herein, Young's modulus through static analysis is calculated and the size effect on the accuracy of 4 CG models is investigated. Then, longitudinal vibrations of the nanowire are studied.

3.1.1. Calculating Young's modulus

Young's modulus is calculated based on the potential energy changes followed by strain changes. For this purpose, five different strains are applied to the nanowire, and variations of the potential energy per unit volume are calculated for these strains as follows

$$\Delta u = \frac{1}{2} E \varepsilon^2 \tag{3.1}$$

where Δu stands for potential energy changes per volume, E is Young's modulus and ε is the strain. By fitting a quadratic curve to the data, Young's modulus is calculated. Figure 4 shows the results for a gold nanowire with $56a_{AA}$ in length and $14a_{AA}$ in thickness.

According to the relative error of the CG models, the most accurate model is the fourth model, which is predictable due to more corrections applied to bead masses and potential parameters in this model. Furthermore, as it is expected, the errors of the first and second CG models are the same. In fact, in static simulations, the mass distribution plays no significant role, and the difference between the first two models and two other models is only because of the distinct potential parameter of the beads. Next, Young's modulus is calculated for different sizes of nanowires and the accuracy of these 4 CG models is examined.

Nanowires with thickness of $14a_{AA}$ and with various lengths are considered for checking the effect of length. The length of these nanowires varies from 4 to 10 times larger than their thicknesses. The results of these simulations show that the error of the CG models is approximately constant for different lengths. Since there is no change in the surface effects by changing length of the nanowire, it is expected that the error of the models does not change significantly with variations of the length.

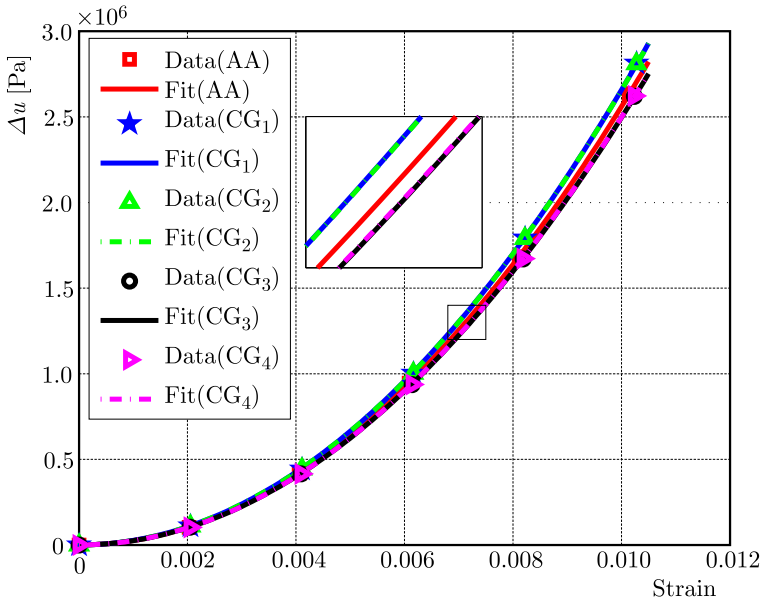

Fig. 4. Variations of the potential energy per volume with respect to strain for a gold nanowire with length of $56a_{AA}$ and thickness of $14a_{AA}$

Thickness is another size parameter influencing the error of the models. The nanowire length is set to be 8 times larger than its thickness. The results depict that the error of the CG models in the prediction of Young's modulus decreases as the nanowire thickness increases. The reason for this behavior is that the surface effects decrease as the nanowire thickness increases. The first and second models use the same potential parameters. Nevertheless, their mass assignments are different. Therefore, it is expected that their behavior in the static and dynamic simulations are similar and different, respectively. Since in this Section a static simulation is performed, the results of these two methods are the same.

3.1.2. Calculating the natural frequency of longitudinal vibration

Here we aim at the investigation of the size effect on the exactness of the proposed CG models in the estimation of the dynamic behavior of the nanowires in longitudinal vibrations. In this regard, the effect of length, thickness, and the scaling parameter on the first longitudinal vibrational frequency of the clamped-free gold nanowire is studied. The details of simulation setup are explained as follows:

- After minimization, two lattices (one lattice in the CG models) at one end of the nanowire are fixed and temperature of the nanowire is maintained at 0.01 K employing the Nosé-Hoover thermostat (Nosé, 1984; Hoover, 1985). It should be mentioned that the higher the temperature of the system is, the greater its kinetic energy is, that may yield incorrect results. Therefore, the nanowire temperature is controlled at 0.01 K.
- The other end of the nanowire is displaced with a constant speed. This displacement is about 1% of the nanowire length to avoid nonlinearity and plastic deformation.
- Then the excited atoms are fixed (at a new position), and temperature of the nanowire is controlled at 0.01 K.
- At the last stage, the end of the nanowire is released to vibrate freely. The corresponding frequency of longitudinal vibrations can be calculated by fitting a sinusoidal function to its end-point displacement (Pishkenari *et al.*, 2015, 2016).

Figure 5 shows the x position of the nanowire free end for a nanowire with length of $80a_{AA}$ and thickness of $20a_{AA}$. According to Fig. 5, all CG methods similar to the AA model pre-

dict oscillating behavior for motion of the nanowire free end. The natural frequencies that are calculated from Fig. 5 are listed in Table 2.

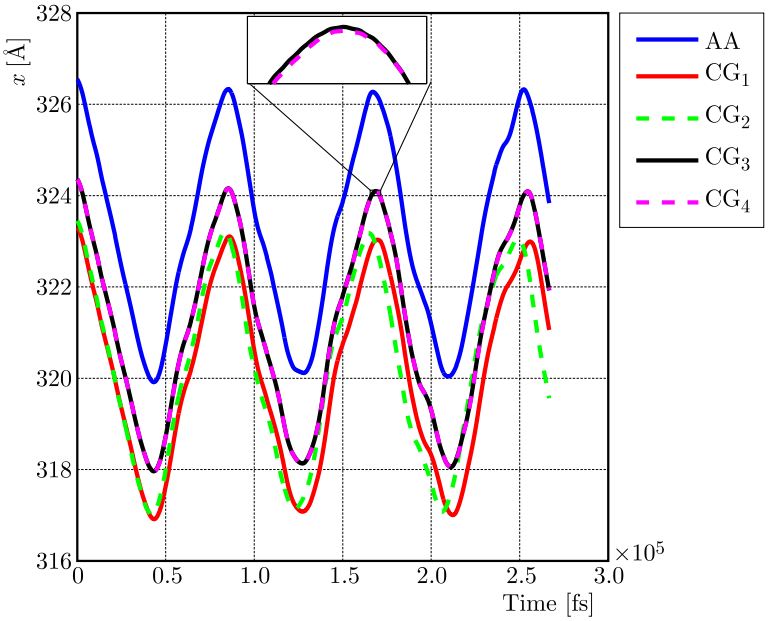

Fig. 5. Position x of the nanowire free end in the fourth step of simulation. The nanowire length and thickness are $80a_{AA}$ and $20a_{AA}$, respectively

Table 2. Natural frequency of longitudinal vibrations for the proposed CG models and the relative error in the estimation of the natural frequency in addition to computation time

	AA	CG_1	CG_2	CG_3	CG_4
Longitudinal natural frequency [GHz]	75.4	74.8	77.1	75.1	75.1
Relative error [%]	—	0.80	2.3	0.40	0.40
CPU time [s]	15356	2021	3666	3832	3917

Based on the relative error of the CG models, the most accurate models are the third and fourth ones. Despite the fact that we expect the error of the second model to be smaller than the first one, the first model is more accurate in this simulation setup. It should be mentioned that the error of the CG models highly depends on the nanowire thickness, and the dependency is different in four CG models. It is worthy to note that functionality of the first, third and fourth CG models on the size parameters of the nanowire is nearly similar (where always the third and fourth models are more precise than the first one), but behavior of the second model is completely distinct. In fact, for a considerable range of nanowire thickness, the second model may give less exact results with respect to the first model (follow the next Sections).

Further simulations are done to investigate the effect of the size parameters on the error of the CG models. Length, thickness and scale parameter are the three size parameters that their effects are studied in this Section.

Length effect: In the simulations, the nanowire length is changed from $48a_{AA}$ to $120a_{AA}$ while its thickness is set as $12a_{AA}$. The results show that the nanowire length does not influence the accuracy of four CG models. This behavior is due to the fact that the surface effects do not significantly change with the nanowire length. A striking point observed in this figure is that at this nanowire thickness the second model is the most precise one.

Thickness effect: Figure 6 illustrates the effect of thickness on the precision of the CG models. In Fig. 6a, the nanowire thickness is varied from $8a_{AA}$ to $20a_{AA}$ and its length is set to be 10 times larger than its thickness. In Fig. 6b, the nanowire length is set to be $100a_{AA}$ and its thickness is varied from $8a_{AA}$ to $20a_{AA}$.

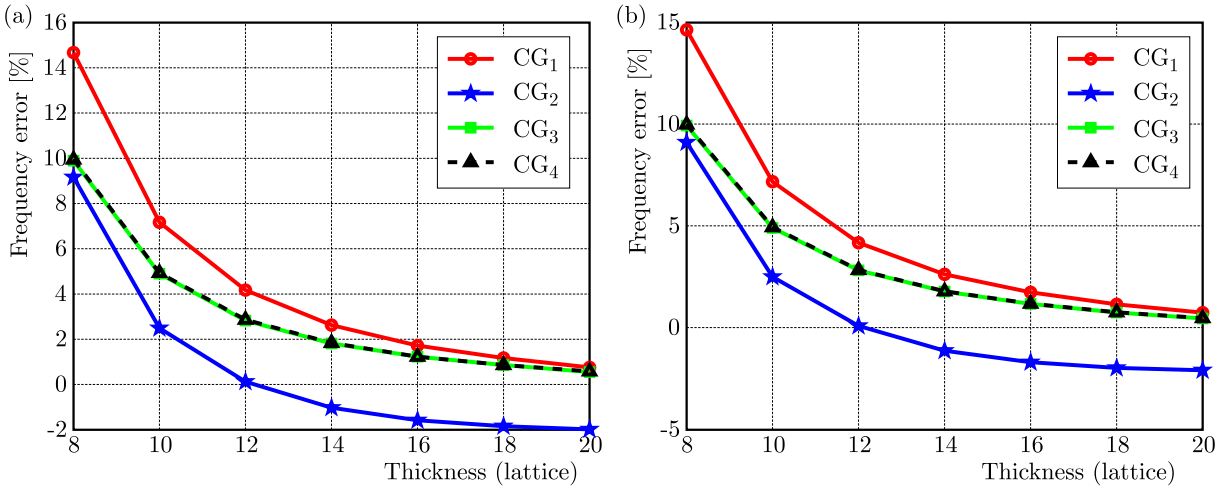

Fig. 6. Error of the estimated longitudinal first natural frequency of the gold nanowire for different CG models: (a) length of the nanowires is 10 times larger than its thickness, (b) nanowire length is set as $100a_{AA}$

Based on Fig. 6, the error of the CG models in the prediction of the longitudinal natural frequency decreases to zero by increasing thickness of the nanowire. The reason for this behavior is that the surface effects reduce as nanowire thickness increases. It should be noted that the second model cannot properly predict the natural frequency for nanowire thicknesses over $14a_{AA}$. In this model, the exterior beads have different masses with respect to the interior beads, while the potential parameters of all beads are the same. Due to limitations in computational facilities, simulations of larger nanowires are not possible in this work. However, for larger thickness, it is expected that the error of the second model converges to zero because all coarse-grained models behave similar to bulk materials.

Scale parameter effect: To examine another effect of nanowire size on the accuracy of the CG models, a nanowire with length of $40a_{AA}$ and thickness of $8a_{AA}$ is considered as the base nanowire, and all of its dimensions are multiplied by a scale parameter. The results show that the frequency error decays to zero for three of the CG models. It should be noted that the surface--to-volume ratio reduces as the nanowire size increases, hence the surface effects should vanish for larger values of the scale parameter. For the second CG model, at first the frequency error descends from positive values to negative values and then it ascends gradually. It is expected that the error of the second model eventually converges to zero for larger values of the scale parameter because the bulk simulations proved that all of the CG models behave as same as the AA model. It should be mentioned that our computational facilities limit our simulations to scale parameter 4.

3.2. Transversal vibrations

In this Section, transversal vibration of the nanowire is investigated. The nanowire free end is displaced and released in the z direction. By fitting a sinusoidal function on motion of this point in the direction of excitation, the transversal natural frequency is measured (Pishkenari *et al.*, 2016). The initial displacement of the beam is equal to 1% of the total nanowire length to avoid large-displacement nonlinear effects. Herein, we will examine the effect of nanowire length and thickness as well as the scale parameter on the accuracy of four CG models.

Length effect: for investigating this effect, a nanowire with thickness of $16a_{AA}$ is considered and its length is varied from $64a_{AA}$ to $160a_{AA}$. As previously discussed, the surface effect does not change with variation of the nanowire length, hence the error of the models remains approximately constant as the nanowire length is altered in these simulations.

Thickness effect: in this Section, the effect of nanowire thickness is studied. The thickness of the nanowire varies from $8a_{AA}$ to $20a_{AA}$. The length of the nanowire for simulations in Figs. 7a and 7b are set to be 10 times larger than the nanowire thickness and $100a_{AA}$, respectively.

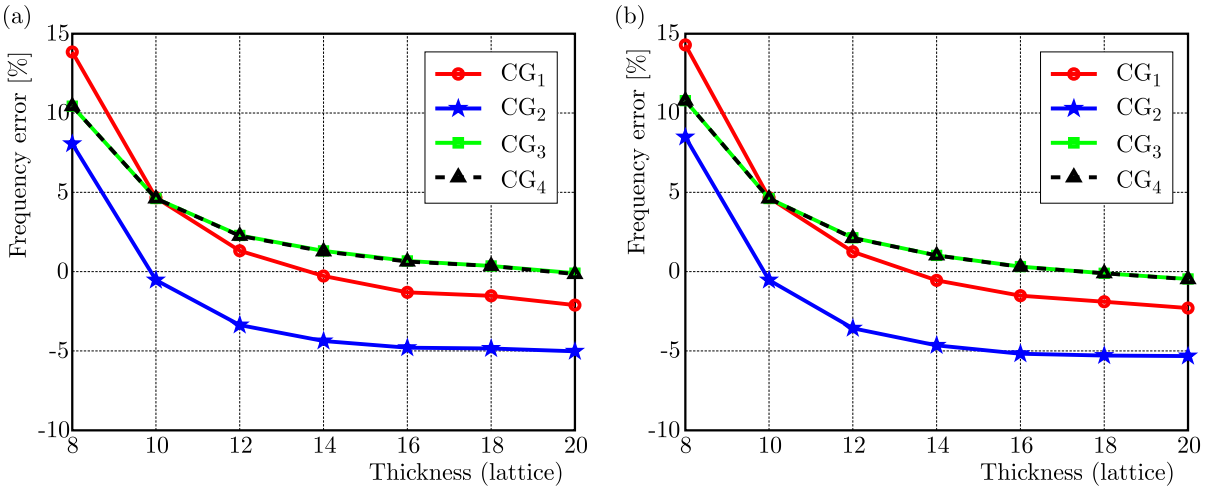

Fig. 7. The error of 4 CG models in estimating the transversal natural frequency as a function of nanowire thickness: (a) length of the nanowire is 10 times larger than its thickness, (b) nanowire length is set to be $100a_{AA}$

Increasing the thickness decreases the surface effect and, therefore, the error of the CG models decays to 0. It should be noted that the error of the first and second CG models does not converge to zero at this thickness interval. However, based on the results of bulk materials, it is expected that the error of these models eventually converges to zero for larger values of the nanowire length whose simulation is beyond capability of our computational resources.

The scale parameter effect: the effect of the scale parameter on the accuracy of the CG models is investigated here. The base nanowire in these simulations has length of $40a_{AA}$ and thickness of $8a_{AA}$. According to the results, the error of the CG models at first descends from positive values to negative values and then slowly ascends. As the nanowire size increases, its properties become closer to behavior of the bulk material. Consequently, the error of the CG models should eventually converge to zero for larger values of the scale parameter. Totally, the third and fourth models have the least error. In this part, the natural frequency of a nanowire with $160a_{AA}$ in length and $32a_{AA}$ in thickness is evaluated. The AA model for the nanowire has more than 670000 atoms, however, the CG model of the nanowire has less than 90000 beads. According to the dimension of the nanowire, approximately 3 million steps are needed to calculate the natural transversal frequency of the nanowire. It causes a seventeen-day simulation for the AA model. Our model can decrease the time to about 4 days while its error is less than 0.6%. When nanowire size rises, not only the number of the beads increases, but also steps of simulations go up. Hence, evaluating the natural frequency for a larger-size nanowire by the AA model is very time-consuming and it is not possible for us to compare our results for larger-size nanowires. Nevertheless, the CG models are capable of modeling these nanowires.

4. Conclusions

In this paper, 4 different CG models are introduced:

1. CG model with one type of bead and one type of potential parameter.
2. CG model with four types of bead and one type of potential parameter.
3. CG model with four types of bead and four types of potential parameter.
4. CG model with eight types of bead and eight types of potential parameter.

To reveal the ability of the CG models for reproduction of results of the original atomic system, we have conducted different simulations. At first, it is shown that these models can predict behavior of the bulk material, including elastic constants, bulk modulus and potential energy, exactly as same as the AA model. Then we have applied longitudinal and transversal displacements to the free end of a nanowire and compared Young's modulus as well as the longitudinal and transversal vibrational frequency of the CG models with the AA model. The results exhibit that the CG models can properly estimate the results of the AA model. Nevertheless, the accuracy of the proposed CG models in calculating mechanical properties of the nanowire highly depends on the nanowire size.

Totally, among four proposed CG models, the error of the second model highly and nonlinearly depends on the nanowire size. Also the error of the second model at a considerable size interval is relatively larger than in other models. The simulation results of the third and fourth models are approximately the same but the third method is slightly faster. These two models are the most accurate models. The error of these models in prediction of the longitudinal and transversal frequencies for nanowires with thickness more than $18a_{AA}$ is less than one percent, while they accelerate the simulations 4 to 8 times. Therefore, the best proposed CG model is the third one. Although the accuracy of the first model is less than in the third model, it is approximately 2 times faster. Therefore, in some cases where speed is more important than accuracy, the first model can be used.

References

1. Berg B.A., 2005, Introduction to Markov chain Monte Carlo simulations and their statistical analysis, *Markov Chain Monte Carlo, Lecture Notes Series*, **7**, 1

2. Burbery N., Das R., Ferguson W., 2017, Dynamic behaviour of mixed dislocations in FCC metals under multi-oriented loading with molecular dynamics simulations, *Computational Materials Science*, **137**, 39-54

3. Cascella M., Dal Peraro M., 2009, Challenges and perspectives in biomolecular simulations: from the atomistic picture to multiscale modeling, *CHIMIA International Journal for Chemistry*, **63**, 14-18

4. Chandramouli P.N., 2014, *Continuum Mechanics*, Yes Dee Publishing Pvt Ltd.

5. Chen Y., Zimmerman J., Krivtsov A., McDowell D.L., 2011, Assessment of atomistic coarse-graining methods, *International Journal of Engineering Science*, **49**, 1337-1349

6. Cranford S., Buehler M.J., 2010, *Coarse-Graining Parameterization and Multiscale Simulation of Hierarchical Systems. Part I: Theory and Model Formulation*, DTIC Document

7. Hedrih K.R.S., Hedrih A.N., 2010, Eigen modes of the double DNA chain helix vibrations, *Journal of Theoretical and Applied Mechanics*, **48**, 219-231

8. Hoover W.G., 1985, Canonical dynamics: equilibrium phase-space distributions, *Physical Review A*, **31**, 1695

9. Jovanovic A.S., Filipovic N., 2006, Innovative modeling methods in damage assessment: application of dissipative particle dynamics to simulation of damage and self-healing of polymer-coated surfaces, *Journal of Theoretical and Applied Mechanics*, **44**, 637-648
10. Karma A., Tourret D., 2016, Atomistic to continuum modeling of solidification microstructures, *Current Opinion in Solid State and Materials Science*, **20**, 25-36
11. Lao J., Tam M.N., Pinisetty D., Gupta N., 2013, Molecular dynamics simulation of FCC metallic nanowires: a review, *JOM*, **65**, 175-184
12. Leach A.R., 2001, *Molecular Modelling: Principles and Applications*, Pearson education
13. Marrink S.J., Risselada H.J., Yefimov S., Tieleman D.P., de Vries A.H., 2007, The MARTINI force field: coarse grained model for biomolecular simulations, *The Journal of Physical Chemistry B*, **111**, 7812-7824
14. Muc A,, 2011, Modelling of carbon nanotubes behaviour with the use of a thin shell theory, *Journal of Theoretical and Applied Mechanics*, **49**, 531-540
15. Nosé S., 1984, A unified formulation of the constant temperature molecular dynamics methods, *The Journal of Chemical Physics*, **81**, 511-519
16. Oren E., Yahel E., Makov G., 2016, Dislocation kinematics: a molecular dynamics study in Cu, *Modelling and Simulation in Materials Science and Engineering*, **25**, 025002
17. Ouldridge T.E., 2012, *Coarse-Grained Modelling of DNA and DNA Self-Assembly*, Springer
18. Paćko P., Uhl T., 2011, Multiscale approach to structure damage modelling, *Journal of Theoretical and Applied Mechanics*, **49**, 243-264
19. Park H.S., Klein P.A., 2007, Surface Cauchy-Born analysis of surface stress effects on metallic nanowires, *Physical Review B*, **75**, 085408
20. Pishkenari H.N., 2015, Atomic interactions between metallic tips and surfaces in NC-AFM, *Journal of Physics D: Applied Physics*, **48**, 125301
21. Pishkenari H.N., Afsharmanesh B., Akbari E., 2015, Surface elasticity and size effect on the vibrational behavior of silicon nanoresonators, *Current Applied Physics*, **15**, 1389-1396
22. Pishkenari H.N., Afsharmanesh B., Tajaddodianfar F., 2016, Continuum models calibrated with atomistic simulations for the transverse vibrations of silicon nanowires, *International Journal of Engineering Science*, **100**, 8-24
23. Pishkenari H.N., Meghdari A., 2010, Surface defects characterization with frequency and force modulation atomic force microscopy using molecular dynamics simulations, *Current Applied Physics*, **10**, 583-591
24. Plimpton S., 1995, Fast parallel algorithms for short-range molecular dynamics, *Journal of Computational Pphysics*, **117**, 1-19
25. Poursina M., Anderson K.S., 2014, An improved fast multipole method for electrostatic potential calculations in a class of coarse-grained molecular simulations, *Journal of Computational Physics*, **270**, 613-633
26. Samani M., Pourtakdoust S.H., 2014, Analysis of two-stage endo-atmospheric separation using statistical methods, *Journal of Theoretical and Applied Mechanics*, **52**, 1115-1124
27. Simmons G., Wang H., 1971, *Single Crystal Elastic Constants and Calculated Aggregate Properties*, 2nd ed., Cambridge, Mass., M.I.T. Press
28. Tadmor E., Legoll F., Kim W., Dupuy L., Miller R., 2013, Finite-temperature quasi-continuum, *Applied Mechanics Reviews*, **65**, 010803, 2013
29. Yang S., Qu J., 2014, An investigation of the tensile deformation and failure of an epoxy/Cu interface using coarse-grained molecular dynamics simulations, *Modelling and Simulation in Materials Science and Engineering*, **22**, 065011

30. Yang Q., To A.C., 2015, Multiresolution molecular mechanics: A unified and consistent framework for general finite element shape functions, *Computer Methods in Applied Mechanics and Engineering*, **283**, 384-418

31. Zhou X., Johnson R., Wadley H., 2004, Misfit-energy-increasing dislocations in vapor-deposited CoFe/NiFe multilayers, *Physical Review B*, **69**, 144113

Manuscript received January 1, 2017; accepted for print September 25, 2017